Materials Science & Engineering A 611 (2014) 388–393

Contents lists available at ScienceDirect

Materials Science & Engineering A

journal homepage: www.elsevier.com/locate/msea

Effect of dislocation density on improved radiation hardening resistance of nano-structured tungsten–rhenium

David E.J. Armstrong *, T.B. Britton [1]

Department of Materials, University of Oxford, Parks Road, Oxford OX1 4JF, United Kingdom

ARTICLE INFO

Article history:
Received 22 May 2014
Received in revised form
2 June 2014
Accepted 4 June 2014
Available online 12 June 2014

Keywords:
Nuclear fusion
Tungsten–rhenium
Nanoindentation
EBSD
Ion implantation

ABSTRACT

Rolled tungsten 5 wt% rhenium sheet has been annealed to produce two microstructures. As received with a high dislocation density, measured using HR-EBSD, and pancake shaped grains with a thickness of ≈200 nm and annealed with equiaxed grains with average grain size of ≈90 μm and low dislocation density. Both materials were ion implanted with 2 MeV W+ ions to damage levels of 0.07, 0.4, 1.2 and 13 displacements per atom (dpa). Nanoindentation was used to measure change in hardness after implantations. While irradiation induced hardening is seen to saturate in the as received material at an increase of 0.4 GPa at 0.4 dpa, the relative hardness change is over four time higher in the annealed material (1.3 GPa) and saturation does not occur by 13 dpa. These differences in radiation response are due to the increased sinks for damage in the as received microstructure in the form of dislocation networks. This is advantageous for use of such nanostructured tungsten sheet in composite materials for structural applications as they will have improved radiation resistance as compared to bulk tungsten products. As well as showing the danger of using idealized microstructures for radiation damage studies.

1. Introduction

Tungsten and its alloys are considered the mostly likely materials for use as plasma facing components in the main chamber and the divertor of future commercial scale nuclear fusion tokamaks such as DEMO [1,2]. This environment is amongst the most challenging to operate in due to high temperatures and irradiation by both 14 MeV neutrons and other charged and neutral particles. Tungsten is the leading candidate material due to its excellent performance at high temperature, including good sputtering resistance and low activation.

All materials subjected to ~14 MeV neutron fluxes in a fusion device will undergo two major physical processes: transmutation and ballistic damage. These result in compositional and microstructural changes and will affect mechanical properties of the base alloy over the lifetime of the component. For pure tungsten it has been predicted by Gilbert and Sublet [3] that after 5 years at DEMO full power operation it would be transmuted to an alloy with the composition W–3.8 at%Re–1.4 at%Os. Such changes in composition have been shown to increase the hardness of the tungsten alloy [4,5] after irradiation with either ions or neutrons as compared to pure tungsten. In addition to transmutation, ballistic neutron damage causes the formation of dislocation loops by the coalescence of point defects which may affect glissile dislocation motion (i.e. slip) [6] and also this damage may result in radiation induced clustering of transmutation products and the formation of non-equilibrium phases [7].

Neutron damage is widely simulated through the use of ion implantation experiments [8], to reducing cost, rapid accumulation of damage and by providing non active samples for post implantation study. However the ion-damage depth is typically on the order of 100 nm to 10 μm. While this is suitable for examination of dislocation structures using transmission electron microscopy [9] and chemical segregation using atom probe tomography [7], the mechanical properties of this thin layer cannot be tested using conventional means, as it is almost impossible to separate the performance of this thin surface layer from the bulk 'substrate' behavior of the unimplanted region. Small scale mechanical testing, often with nanoindentation, has previously provided mechanical data for a range of ion implanted layers [4,10–16].

Previous work Armstrong et al. [4] using large grained annealed pure tungsten and large grained annealed tungsten–rhenium alloys and implantation with 2 MeV W+ ions to damage levels from 0.04 dpa to 33 dpa has been shown to cause the formation of small (2–10 nm) prismatic dislocation loops. A significant increase in hardness [4], measured with nanoindentation, attributed to the interaction between loops and dislocations, has been observed, even at the lowest damage levels. Observation of defects with electron microscopy techniques as well as mechanical testing with

* Corresponding author.
E-mail address: david.armstrong@materials.ox.ac.uk (D.E.J. Armstrong).
[1] Current address: Department of Materials, Imperial College, London SW7 2AZ, United Kingdom.

http://dx.doi.org/10.1016/j.msea.2014.06.013
0921-5093/

nanoindentation reveals structures and behaviors which are similar to damage accumulation and hardness increase trends seen in tungsten and tungsten rhenium alloys irradiated using neutrons and studied using micro-indentation [17,18].

As discussed above the performance of tungsten at elevated temperatures is certainly lauded for in-reactor operations, yet this makes fabrication of complex large parts very taxing (as forming processes are very difficult due to the inherent brittleness of bulk tungsten and its high melting point). This will also introduce difficulties during plant construction and has safety implications for the handling of irradiated parts during shutdown periods and plant decommissioning. Fundamentally, the brittle to ductile temperature (BDTT) of bulk samples of pure tungsten is between 120 and 250 °C [19] depending on strain rate, with little success seen in reducing this by alloying alone [20]. However this temperature can be reduced by clever materials design, with recent work by Reiser et al. [21–24] offering much promise. They show that one option for manufacture of such components is to join thin tungsten foils (thickness ≈ 100 μm) with a copper brazing braze to form hybrid alloy/composite laminate structures millimeters in dimension, such as a prototype tungsten pipe [22]. In addition, the complex microstructure results in an impressive reduction of 500 °C on the brittle to ductile transition temperature.

Foils used in this process are produced by rolling from bulk tungsten which results 'nanostructured' materials with fine grains sizes and high dislocation densities [21]. As discussed by Wurster and Pippan [25] nanostructured materials are generally considered to have superior radiation resistance due to the large number of interfaces which can act as sinks for the defects produced by irradiation, however experimental evidence for this is sparse, and no data is currently available for nanostructured tungsten.

Sharma et al. [26,27] investigated changes in hardness of nanocrystalline nickel after irradiation by protons and helium ions. Even at very low damage levels (0.004 dpa) produced by proton implantation a significantly (although unquantified) larger increase in hardness is seen for bulk nickel as compared to nanocrystalline nickel implanted to the same damage level. This is attributed to extra grain boundary volume in the nc-Ni acting as efficient sinks. After implantation with He+ ions the hardness of nc-Nickel increased from 2.9 GPa to 3.7 Gpa, however in this case it is unclear what the mechanisms for hardness increase will be as while both dislocation loops and helium-vacancy clusters, which can have a significant hardening effect [28], will be present and unfortunately Sharma et al. do not present any information on the location of the helium. Pouchon et al. [29] performed He+ ion implantation, to a damage level of ≈1 dpa, on two PM2000 ODS steel samples, one with nano-crystalline grains produced by severe plastic deformation and a second heat treated to produce a significantly coarser grain size. No differences between the irradiation hardening in the two materials was observed using nanoindentation. This suggests rather than the boundary volume acting as the predominant sink site, that the ODS particles or internal dislocations act as sinks themselves. Another nanostructured class of materials discussed with potential for high radiation resistance is nanolaminates. In work by Demkowicz et al. [30] alternating layers of Cu and Nb were shown to be highly effective sinks for radiation induced point defects. Such nanolaminates have been suggested for use in advanced nuclear systems, but scaling up such systems to the sizes required for structures in divertors will prove challenging. Tungsten with a nano-structured grain morphology and high dislocation density can be produced by several different plastic deformation routes, including high pressure torsion [31] and rolling [21]. In particular rolling can produce materials which can be layered together with the potential to produce bulk components, as shown by the manufacture of a basic tungsten foil pipe by Reiser et al. [22]. This offers an attractive route for manufacturing bulk tungsten components with a nanostructured microstructure.

Thus understanding how the mechanical properties of such nanocrystalline tungsten foils are affected by irradiation damage is vital to the successful development of foil-composite materials, as well as understanding how the cascade damage effects mechanical properties in non-ideal microstructures.

2. Materials and methods

In this study W–5 wt%Re foil (Plansee, Austria) has been used, which has a very similar microstructure to pure tungsten foil (BCC, with Re in solid solution). The chemical composition has been selected to be similar to that expect after 5 years in a DEMO type 14 MeV neutron spectrum [3].

Foils were rolled to a thickness of 250 μm by Plansee, Austria, using a proprietary rolling method. Foils were sectioned into pieces approximately 10 mm × 20 mm, half of these were annealed for 24 h at 1400 °C in vacuum.

These foils were studied using conventional (hough) and cross-correlation based EBSD to reveal maps of grain structure and dislocation densities respectively, with excellent spatial resolution across many grains [33,42]. The high resolution EBSD variant compares two or more diffraction patterns to generate maps of misorientation (and elastic strain) variation with respect to a reference pattern within each grain.

In this study we have used these high angular resolution misorientation maps (~1E-4 rads) to calculate stored geometrically necessary dislocation density maps, using the Nye tensor [32]. Briefly, arrays of dislocations with a net Burgers vector will result in lattice curvature. This curvature can be measured and related back to specific dislocation types using knowledge of the likely families of active slip systems and crystal orientation of the grain. Unfortunately there are often more than slip systems than curvatures measured and so we have used a L1 minimization scheme which results in a dislocation density at each point that supports the measured curvature and utilized slip systems which result in a configuration with the lowest line energy. We present our results as a simple scalar sum of the total dislocation density. The high resolution variant enables GND densities to be calculated with a significantly lower noise floor (ρ_{min} dθ/b * xstep) [42]. For more details on this method, readers are directed to a recent overview [33].

EBSD was conducted using a JEOL JSM-6500F at 30 kV with a 50 nm step size. GND densities were calculated using only {110}⟨111⟩ type systems, with L1 weighting based upon line energy that differs for edge and components.

W+ ion implantation was performed out at the Surrey National Ion Beam Centre, University of Surrey, UK. Samples in each condition were mechanically mounted on a stainless steel plate, allowing part of each sample to be blanked from the beam, and heated to 300 °C, monitored using a thermocouple mounted alongside the samples, as described elsewhere [6,10,4]. W+ ions were implanted at 2 MeV using a tandem accelerator, at doses of 5.5×10^{16} W^+ ions/m^2 to 1.9×10^{19} W^+ ions/cm^2. Using SRIM [34] (stopping range of ions in matter) the expected damage profile and level was calculated and converted into displacement per atoms (dpa), assuming a binding energy of 68 eV [35]. The damage occurred over a range of ≈200 nm with the peak damage level occurring at ≈100–125 nm. The lowest dose corresponded to a peak damage level of 0.07 dpa and the highest of 13 dpa.

Nanoindentation was carried out using a MTS Nano Indenter XP (MTS, TN, USA) with continuous stiffness measurement (CSM) [36] and a diamond Berkovich indenter tip allowing the measurement of hardness as a function of indentation depth. 32 indents

were made in each sample 16 in the implanted and 16 in the unimplanted region all to a depth of 1000 nm, to ensure the indent was made significantly deeper than the predicted damage profile. The difficulties in measuring the mechanical properties of ion implanted layers without being dominated by underlying unimplanted material have been discussed extensively elsewhere. Previous work by Armstrong et al. [4] using a method developed for studying coated systems has shown that that for this combination of tungsten and 2 MeV W^+ ions a hardness value taken at 125 nm allows comparisons between samples without either surface effects or the underlying unplanted material obscuring or dominating the results.

3. Results

EBSD of representative regions of the rolled and annealed samples are show in Fig. 1a and b. These maps reveal that are significant differences in the morphology of the rolled and annealed samples. The rolled sample (Fig. 1a) is largely red and therefore has a strong {001} texture component. Within these grains, there is significant sub-grain structure which is common to other BCC metals. In the annealed case, the grains are significantly larger, the texture is much less strong and there is less intragranular misorientation (i.e. Color gradients). The {001} pole figure maps,1 c and d confirm that the out of plane texture is very strong and that the in plane $<001>$ directions point along the subgrain boundaries in the rolled structure. The annealing texture is less strong than the rolled texture and shows that the texture has largely split into two – with two central peaks and a $\sim 15^\circ$ rotation for the in plane $<001>$ directions.

The ion-channeling induced secondary image from a FIB cross section shown in Fig. 1e reveals a pancake grain structure consistent with the rolling of ~equiaxed grains, the grain thickness is $\approx$75–200 nm. Again this is as expected for rolled BCC metals and the aspect ratio is consistent with the appropriate reduction in thickness for the rolled sheet. Fig. 2 shows grain diameter histograms for the two samples, on annealing the average grain diameter (rolled plane) increases from $\approx 2\,\mu m$ to close to $\approx 100\,\mu m$.

To determine the density of geometrically necessary dislocations, maps with less pattern binning were captured (Fig. 3) and

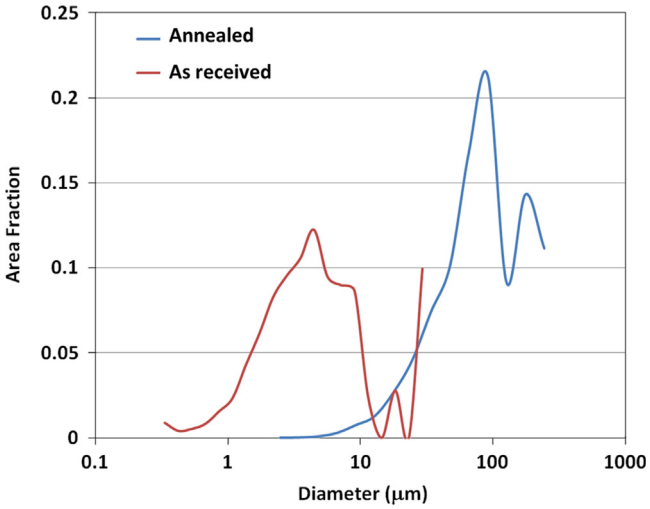

Fig. 2. Grain size distributions for as received and annealed W–5 wt%Re.

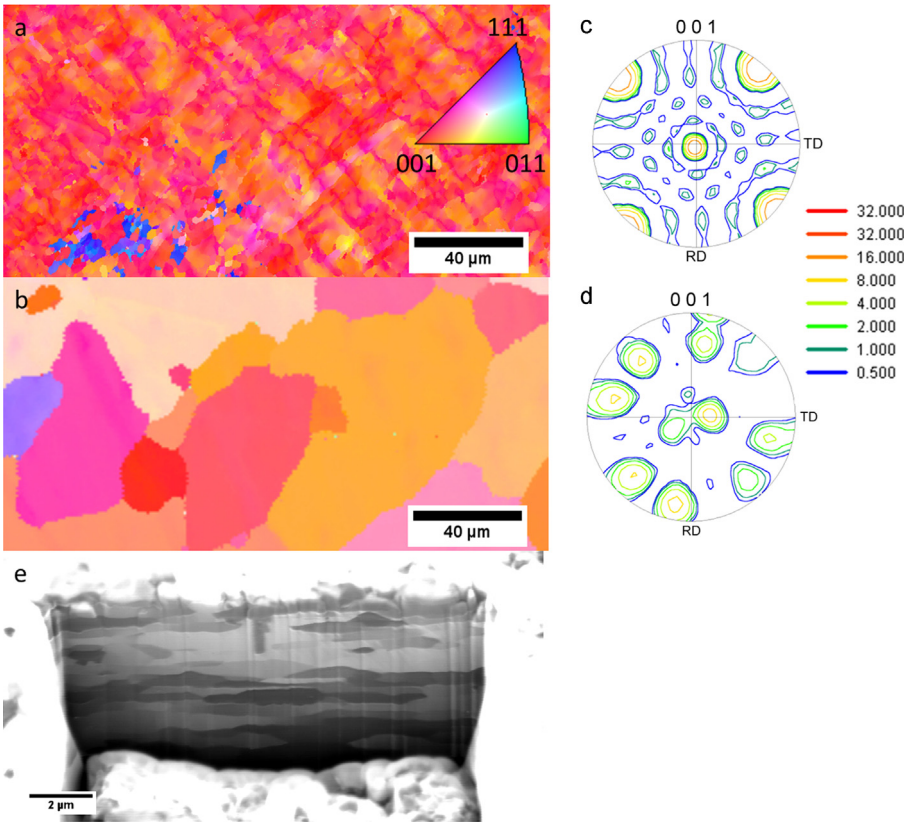

Fig. 1. (a) EBSD IPF map of surface normal crystallography of as received W–5 wt%Re. (b) EBSD IPF map of surface normal crystallography of annealed W–5 wt%Re. (c) 001 pole figure texture map for as received W–5 wt%Re surface normal (d) 001 pole figure texture map for annealed W–5 wt%Re surface normal. (e) FIB-Secondary electron image of cross section of as received W–5 wt%Re showing elongated grains along rolling direction.

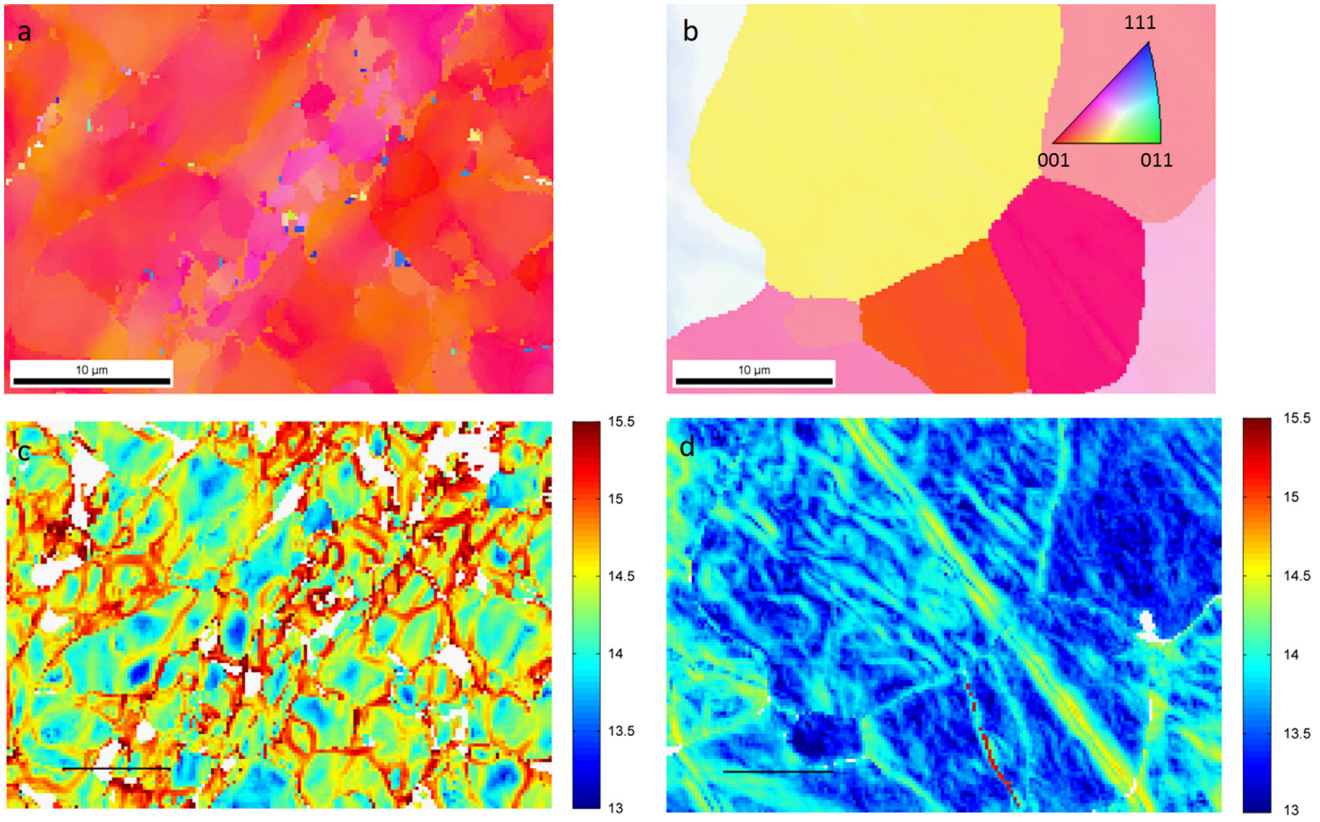

Fig. 3. Higher magnification maps of the two materials (a and b) EBSD IPF map of the surface normal crystallography; (c and d) calculated GND content calculated with the HR-EBSD analysis showing stored dislocation content on a log 10(dislocations per m^2) scale.

for each data point the EBSD pattern was saved to disk. High resolution EBSD analysis was performed to determine the density of geometrically necessary dislocations and the results for the rolled and annealed samples are presented in Fig. 3(c) and (d) respectively.

These maps reveal a stark difference in the stored dislocation content. As indicated in the IPF maps in Fig. 1, color gradients within the rolled sample are due to misorientation gradients that can be linked to subgrain structure and walls of high dislocation content. The sub-grain structures in this sample are typically a few micrometers in size and contain areas of low GND density ($<10^{13}$ per m^2) surrounded by walls a high GND density ($>10^{15}$ per m^2) When the material is annealed, the grains grow and there are significantly fewer and less intense sub-grain boundaries. Quantitative analysis of the data contained within these GND maps has been performed through construction of frequency histograms on a log 10(dislocations per m^2) scale presented in Fig. 4.

These histograms confirm our initial observations, annealing of the material results in a significant reduction in the stored dislocation content, with a (geometric) mean value of 4.8×10^{13}lines/m^2 in the annealed material and 1.4×10^{14}lines/m^2 in the annealed material.

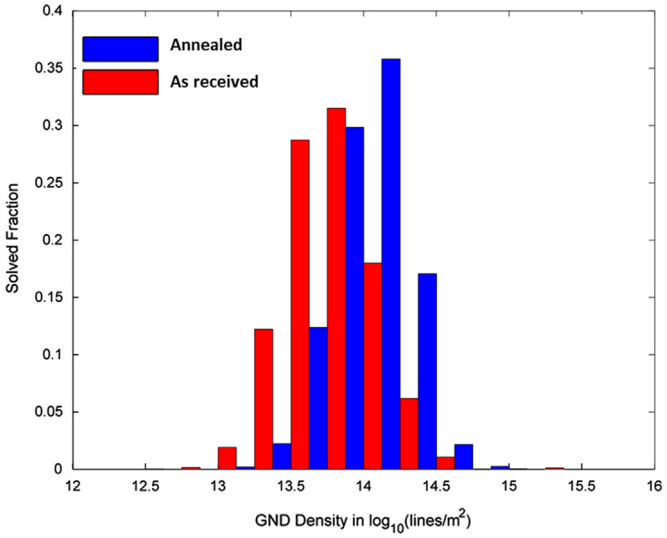

Fig. 4. GND density frequency histograms from Fig. 3(c and d) showing the average defect populations in the two scanned regions.

Fig. 5a shows hardness–displacement curves measured using the CSM technique for both unimplanted and samples implanted to 0.4 dpa. The unimplanted samples in both the as received and annealed condition show a small indentation size effect at shallow indents depths, and the hardness of the as received sample is consistently 2 GPa larger than the annealed, due to both grain growth and reduction in dislocation density after annealing. On irradiation the hardness of both the as received and annealed material is seen to increase. This increase in hardness is seen to be at a maximum at $\approx$80 nm indenter displacement and is negligible by $\approx$500 nm in both material conditions. Fig. 5b and c shows the absolute hardness values and relative changes in hardness values at 125 nm for both material conditions and all five damage levels. In the annealed condition the hardness increases at the lowest irradiated does (0.07 dpa) by 0.8 GPa, (from 6.3 Gpa to 7.1 GPa), further irradiations to higher damage levels shows subsequent increases in hardness, and by 13 dpa damage the hardness has increased by 1.35 GPa to 7.8 GPa. However the increase in hardness as a function of damage level in the unannealed foil is significantly different. After the first irradiation (0.07 dpa) the hardness

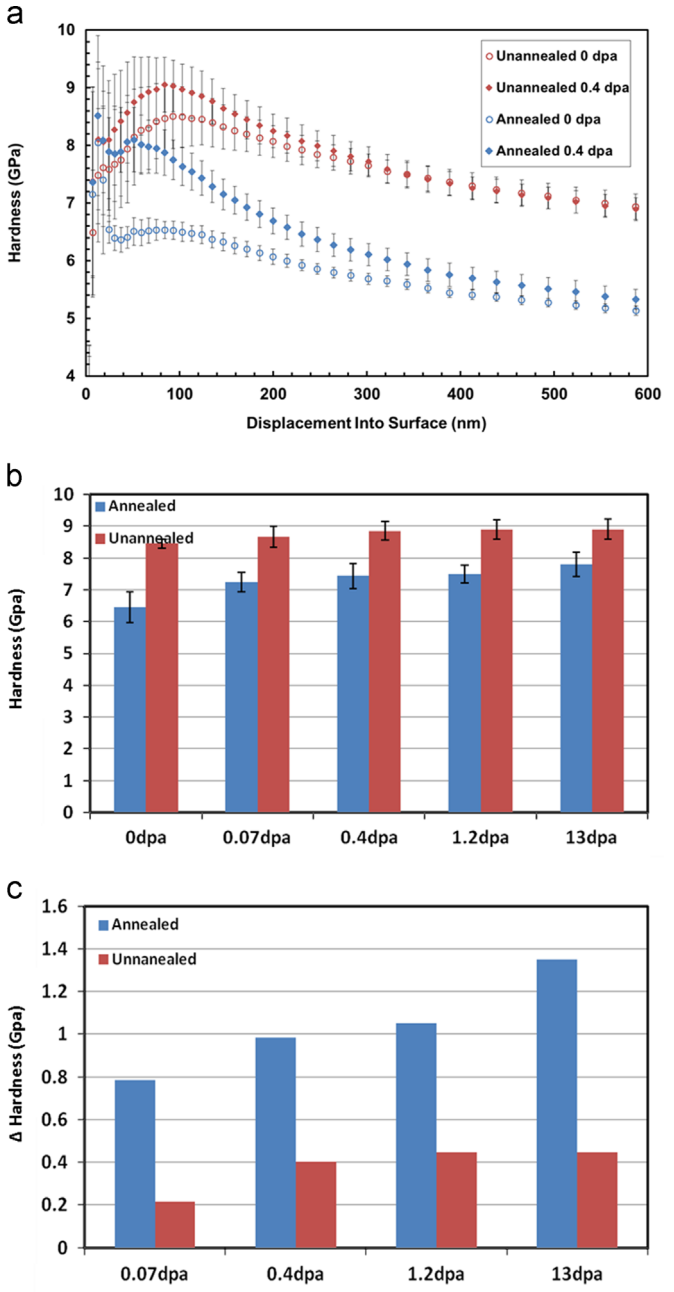

Fig. 5. (a) Hardness vs indenter displacement curves for as received and annealed W–5 wt%Re samples with 0 dpa and 0.4 dpa damage levels. (b) Chart showing absolute hardness values for as received and annealed W–5 wt%Re for all damage levels. (c) Relative hardness changes with respect to 0 dpa samples for as received and annealed W–5 wt%Re for all damage levels. Saturation of hardness increase is seen in the as received but not in the annealed condition.

increases by 0.2 GPa to an absolute value of 8.6 GPa. The following three irradiation conditions the same increase in hardness of 0.4 Gpa, and the hardness increase seems to have saturated.

4. Discussion

The microstructure of rolled pure tungsten changes significantly between rolling and annealing. Clearly this is not surprising. The impact of this microstructure on the micromechanical response, tested here with nanoindentation, is of great significance when considering not only real materials in real environments, but also the extrapolation of ideal materials testing and simulated radiation damage (ion implantation) on mechanical performance.

Armstrong et al. [4] note that there are two competing mechanisms for hardening in the W–Re system after irradiation. These are the damage produced by the production of point defects and subsequent dislocation loops, and the formation of nanoscale clusters of rhenium atoms. Their work has shown under self-ion irradiation at 300 °C there is little formation of precipitates in W–5 wt%Re, up to 13 dpa of self-ion damage. Thus the majority of the hardness increase in this system below 13 dpa damage must be a product of the point defects and dislocation loops produced, i.e. the formation of non-chemical microstructure. The formation of microstructure which can confirm this hypothesis has been performed using both in-situ [37] and post irradiation [4] TEM studies in W–5 wt%Re. In both cases the damage was found to be a mixture of both interstitial and vacancy 1/2 ⟨111⟩ and ⟨100⟩ loops. These studies focused on well annealed samples, yet in real engineering components microstructural defects such as a grain boundaries and existing dislocation structure will act as sinks for radiation damage. As shown by Pouchon et al. [29] materials with a coarse grain size can still show resistance to radiation damage if there is an alternative set of recombination sinks, such as nano-clusters, available. This leads cleanly to the importance and relevance of this study.

Use of rolling and annealing has presented us with the unique opportunity to study the same batch of material with different defect populations. The nano-structure of the rolled material, with areas of significantly high dislocation density, surrounded by cleaner sub-grain interiors, clearly has an impact on the mechanical response. This is not surprising and can briefly be explained through simple forest hardening mechanisms. Here we have gone one step further and subjected these two materials to ion irradiation and clearly demonstrated that the radiation hardening seen is significantly different, even when differences between forest hardening of the worked layer are taken into account. Annealed microstructures tend to over emphasize increases in hardening associated with self-ion implantation.

Prior work in molybdenum can be used to understand our findings. Brimhall and Mastel [38] showed a zone denuded of dislocation loops of width ≈200 nm adjacent to a grain boundary which had been neutron irradiated at 400 °C. Additional work by Li et al. [39] using in-situ 1 MeV Kr irradiation of molybdenum at 80 °C studied the effect of grain boundaries in acting as sinks and hence reducing the number of dislocation loops in their vicinity. They showed a reduction in areal loop density of 64% close to the grain boundary and a significant reduction in areal density up to 30 nm away. Mapping this to the as received W–5 wt%Re studied in this work, the grain size ranges from 0.2–1 μm in thickness (Fig. 1C) and ≈1–10 μm in diameter. This is larger than the denuded zone seen by Li et al. and suggests that grain boundaries are not the dominant sink for point defects.

Rapid crystallographic examination to generate maps of orientation, as performed here, indicates that definition of a grain, and by proxy grain size, may not be sufficient to understand the complex behavior of real materials. In deformed samples there are significant orientation gradients, which render thresh holding of a grain difficult. In the context of radiation damage, we must focus on areas of either higher stored energy, or existing defects, and link these to generation and coalescence of defects during irradiation. High resolution EBSD reveals that there is significant grain substructure, in the form of sub-grain walls of high dislocation density, which must be acting as effecting recombination centers for point defects.

The bulk nature of samples studied here is significant. Cluster dynamics work by Xu et al. [40] has modeled the effectiveness of dislocations as sinks compared to surface effects in TEM

experiments. Surface effects are expected to dominate for in-situ TEM irradiations the dislocations are shown to have a significant effect as sinks for point defects. In bulk W–5 wt%Re where surface effects will not play a role this suggests that regions of high dislocation density will be acting as an even more effective sink for point defects leading to the saturation in hardening seen in nano-structure tungsten 5 wt%Re.

Tungsten used in structural components such as the divertor will be operating at temperatures from up to 700 °C [41], which is below the temperature at which annealing is observed [21] in such foils. Use and maintenance of deformed microstructures which contain sub-grain structures as observed here will result in enhanced radiation resistance improved component lifetime.

5. Conclusions

This work has shown that the resistance to radiation induced hardening in as-rolled nano-structured tungsten rhenium sheet is considerably higher than the resistance of annealed sheet with an average grain size ≈ 50 times larger. This is likely to be due to the larger number of dislocations provided by the nanostructured sheet which will allow for the recombination of vacancies without the formation of new dislocation loops. This is advantageous for use of such nanostructured tungsten sheet in composite materials for structural applications as they will have improved radiation resistance as compared to bulk tungsten products.

Acknowledgments

DEJA thanks Culham Centre for Fusion Energy for funding via a Research Fellowship at St Edmund Hall, Oxford, and The Royal Academy of Engineering for a Research Fellowship at the University of Oxford. DEJA and TBB acknowledge support from EPSRC Grants EP/H018921/1, EP/G004676/1, and EP/F004451/1, and the support of staff at the National Ion Beam Centre, University of Surrey, UK.

References

[1] M. Rieth, J.L. Boutard, S.L. Dudarev, T. Ahlgren, S. Antusch, N. Baluc, M.-F. Barthe, C.S. Becquart, L. Ciupinski, J.B. Correia, C. Domain, J. Fikar, E. Fortuna, C.-C. Fu, E. Gaganidze, T.L. Galán, C. García-Rosales, B. Gludovatz, H. Greuner, K. Heinola, N. Holstein, N. Juslin, F. Koch, W. Krauss, K.J. Kurzydlowski, J. Linke, Ch. Linsmeier, N. Luzginova, H. Maier, M.S. Martínez, J.M. Missiaen, M. Muhammed, A. Muñof, M. Muzyk, K. Nordlund, D. Nguyen-Manh, P. Norajitra, J. Opschoor, G. Pintsuk, J. Nucl. Mater. 417 (2011) 463–467.

[2] M. Rieth, S.L. Dudarev, S.M. Gonzalez de Vicente, J. Aktaa, T. Ahlgren, S. Antusch, D.E.J. Armstrong, M. Balden, N. Baluc, M.F. Barthe, W.W. Basuki, M. Battabyal, C.S. Becquart, D. Blagoeva, H. Boldyryeva, J. Brinkmann, M. Celino, L. Ciupinski, J.B. Correia, A. Debacker, C. Domain, E. Gaganidze, C. García-Rosales, J. Gibson, M. Gilbert, S. Giusepponi, B. Gludovatz, H. Greuner, K. Heinola, T. Höschen, A. Hoffmann, N. Holstein, F. Koch, W. Krauss, H. Li, S. Lindig, J. Linke, C. Linsmeier, P. López-Ruiz, H. Maier, J. Matejicek, T.P. Mishra, M. Muhammed, A. Muñoz, M. Muzyk, K. Nordlund, D. Nguyen-Manh, J. Opschoor, N. Ordás, T. Palacios, G. Pintsuk, R. Pippan, J. Reiser, J. Riesch, S. G. Roberts, L. Romaner, M. Rosiński, M. Sanchez, W. Schulmeyer, H. Traxler, A. Ureña, J.G. van der Laan, L. Veleva, S. Wahlberg, M. Walter, T. Weber, T. Weitkamp, S. Wurster, M.A. Yar, J.H. You, A. Zivelonghi, J. Nucl. Mater. 432 (2013) 482–500.

[3] M.R. Gilbert, J.C. Sublet, Nucl. Fusion 51 (2011) 043005.

[4] D.E.J. Armstrong, X. Yi, E.A. Marquis, S.G. Roberts, J. Nucl. Mater. 432 (2013) 428–436.

[5] A. Hasegawa, T. Tanno, S. Nogami, M. Satou, J. Nucl. Mater. 417 (2011) 491–494.

[6] E.M. Grieveson, D.E.J Armstrong, S. Xu, S.G. Roberts, J. Nucl. Mater. 430 (2012) 119–124.

[7] E.A. Marquis, J.M. Hyde, D.W. Saxey, S. Lozano-Perez, V. de Castro, D. Hudson, C.A. Williams, S. Humphry-Baker, G.D.W. Smith, Mater. Today 12 (2009) 30–37.

[8] G.S. Was, Fundamentals of Radiation Materials Science: Metals and Alloys, Springer, Berlin; New York, 2007.

[9] M.L. Jenkins, J. Nucl. Mater. 216 (1994) 124–156.

[10] D.E.J. Armstrong, A.J. Wilkinson, S.G. Roberts, Phys. Scr. T145 (2011) 014076.

[11] E.M. Grieveson, D.E.J. Armstrong, S. Xu, S.G. Roberts, J. Nucl. Mater. 430 (2012) 119–124.

[12] C. Heintze, F. Bergner, M. Hernandez-Mayoral, J. Nucl. Mater. 417 (2011) 980–983.

[13] C. Heintze, C. Recknagel, F. Bergner, M. Hernandez-Mayoral, A. Kolitsch, Nucl. Instrum. Methods Phys. Res. Sect. B-Beam Interact. Mater. Atoms 267 (2009) 1505–1508.

[14] P. Hosemann, C. Vieh, R.R. Greco, S. Kabra, J.A. Valdez, M.J. Cappiello, S. A. Maloy, J. Nucl. Mater. 389 (2009) 239–247.

[15] R. Kogler, W. Anwand, A. Richter, M. Butterling, X. Ou, A. Wagner, C.L. Chen, J. Nucl. Mater. 427 (2012) 133–139.

[16] A.J. Bushby, S.G. Roberts, C.D. Hardie, J. Mater. Res. 27 (2012) 85–90.

[17] T. Tanno, M. Fukuda, S. Nogami, A. Hasegawa, Mater. Trans. 52 (2011) 1447–1451.

[18] T. Tanno, A. Hasegawa, J.C. He, M. Fujiwara, S. Nogami, M. Satou, T. Shishido, K. Abe, Mater. Trans. 48 (2007) 2399–2402.

[19] A. Giannattasio, Z. Yao, E. Tarleton, S.G. Roberts, Philos. Mag. 90 (2010) 3947–3959.

[20] M. Rieth, S.L. Dudarev, S.M. Gonzalez de Vicente, J. Aktaa, T. Ahlgren, S. Antusch, D.E.J. Armstrong, M. Balden, N. Baluc, M.F. Barthe, W.W. Basuki, M. Battabyal, C.S. Becquart, D. Blagoeva, H. Boldyryeva, J. Brinkmann, M. Celino, L. Ciupinski, J.B. Correia, A. De Backer, C. Domain, E. Gaganidze, C. García-Rosales, J. Gibson, M.R. Gilbert, S. Giusepponi, B. Gludovatz, H. Greuner, K. Heinola, T. Höschen, A. Hoffmann, N. Holstein, F. Koch, W. Krauss, H. Li, S. Lindig, J. Linke, C. Linsmeier, P. López-Ruiz, H. Maier, J. Matejicek, T.P. Mishra, M. Muhammed, A. Muñoz, M. Muzyk, K. Nordlund, D. Nguyen-Manh, J. Opschoor, N. Ordás, T. Palacios, G. Pintsuk, R. Pippan, J. Reiser, J. Riesch, S.G. Roberts, L. Romaner, M. Rosiński, M. Sanchez, W. Schulmeyer, H. Traxler, A. Ureña, J.G. van der Laan, L. Veleva, S. Wahlberg, M. Walter, T. Weber, T. Weitkamp, S. Wurster, M.A. Yar, J.H. You, A. Zivelonghi, J. Nucl. Mater. 432 (2013) 482–500.

[21] J. Reiser, M. Rieth, B. Dafferner, A. Hoffmann, X.O. Yi, D.E.J. Armstrong, J. Nucl. Mater. 424 (2012) 197–203.

[22] J. Reiser, M. Rieth, B. Dafferner, A. Hoffmann, J. Nucl. Mater. 423 (2012) 1–8.

[23] J. Reiser, M. Rieth, A. Möslang, B. Dafferner, J. Hoffmann, T. Mrotzek, A. Hoffmann, D.E.J. Armstrong, X. Yi, J. Nucl. Mater. 436 (2013) 47–55.

[24] P. Norajitra, R. Giniyatulin, V. Kuznetsov, I.V. Mazul, G. Ritz, Fusion Eng. Des. 85 (2010) 2251–2256.

[25] S. Wurster, R. Pippan, Scr. Mater. 60 (2009) 1083–1087.

[26] Garima Sharma, Apu Sarkar, Jalaj Varshney, U. Ramamurty, Ajay Kumard S.K. Gupta, J.K. Chakravartty, Scripta Materialia 65 (2011) 727–730.

[27] Garima Sharma, P. Mukherjee, Arnomitra Chatterjee, N. Gayathri, Apu Sarkar J.K. Chakravartty, Acta Materialia, 61 (2013) 3257–3266.

[28] D.E.J Armstrong, PD Edmondson, SG Roberts, Applied Physics Letters 102 (2013), 251901.

[29] M.A. Pouchon, J. Chen, R. Ghisleni, J. Michler, W. Hoffelner, Experimental Mechanics 50 (2010) 79–84.

[30] M.J. Demkowicz, P. Bellon, B.D. Wirth, MRS Bulletin 35 (2010) 992–998.

[31] M. Faleschini, H. Kreuzer, D. Kiener, R. Pippan, J. Nucl. Mater. 367 (2007) 800–805.

[32] J.F. Nye, Acta Metall. 1 (1953) 153–162.

[33] T. Ben Britton, J. Jiang, P.S. Karamched, A.J. Wilkinson, JOM 65 (2013) 1245–1253.

[34] J.F. Ziegler, M.D. Ziegler, J.P. Biersack, Nucl. Instrum. Methods Phys. Res. Sect. B-Beam Interact. Mater. Atoms 268 (2010) 1818–1823.

[35] A. International, ASTM International, West Conshohocken, PA, 2009.

[36] W.C. Oliver, G.M. Pharr, J. Mater. Res. 7 (1992) 1564–1583.

[37] X. Yi, M.L. Jenkins, M. Briceno, S.G. Roberts, Z. Zhouc, M.A. Kirk, Phil Mag, 93 (2013) 1715–1738.

[38] J.L. Brimhall, B. Mastel, Radiat. Eff. 3 (1970) 203–215.

[39] M.M. Li, M.A. Kirk, P.M. Baldo, D.H. Xu, B.D. Wirth, Philos. Mag. 92 (2012) 2048–2078.

[40] Meimei Li, M.A. Kirk, P.M. Baldo, Donghua Xu & B.D. Wirth Philosophical Magazine 92, (2012).

[41] P. Norajitra, R. Giniyatulin, T. Ihli, G. Janeschitz, W. Krauss, R. Kruessmann, V. Kuznetsov, I. Mazul, V. Widak, I. Ovchinnikov, R. Ruprecht, B. Zeep, Fusion Eng. Des. 82 (2007) 2740–2744.

[42] J Jiang, TB Britton and AJ Wilkinson. Measurement of geometrically necessary dislocation density with high resolution electron backscatter diffraction: Effects of detector binning and step size. Ultramicroscopy (2013), vol. 125, 1-9, http://dx.doi.org/10.1016/j.ultramic.2012.11.003.